Nanoscale

Cell mechanics correlates with resistance to malignant transformation in naked mole rat fibroblasts

Journal:	*Nanoscale*
Manuscript ID	NR-ART-03-2022-001633.R3
Article Type:	Paper
Date Submitted by the Author:	31-Aug-2022
Complete List of Authors:	Makarova, Nadezda; Tufts University Kalaparthi , Vivekanand ; Tufts University Seluanov, Andrei; University of Rochester Gorbunova, Vera; University of Rochester Dokukin, Maxim; Tufts University Sokolov, Igor; Tufts University

Cell mechanics correlates with the resistance to malignant transformation in naked mole rat fibroblasts

Nadezda Makarova[1], Vivekanand Kalaparthi[1†], Andrei Seluanov[2], Vera Gorbunova[2], Maxim Dokukin[1,3,4], Igor Sokolov[1,6,7,]*

[1]Department of Mechanical Engineering, Tufts University, Medford, MA 02155, USA

[3]NanoScience Solutions, Inc., Arlington, VA 22203, USA

[4]Sarov Physics and Technology Institute, MEPhI, Sarov, Russian Federation

[6]Department of Biomedical Engineering, Tufts University, Medford, MA 02155, USA

[7]Department of Physics, Tufts University, Medford, MA 02155, USA

* Email: Igor.Sokolov@Tufts.edu

Abstract

Naked mole rats (NMR) demonstrate exceptional longevity and resistance to cancer. Using biochemical approach, it was previously shown that the treatment of mouse fibroblast cells with RasV12 oncogene and SV40 Large T antigen (viral oncoprotein) led to malignant transformation in cells. In contrast, NMR fibroblasts were resistant to the malignant transformations up on this treatment. Here we demonstrate that atomic force microscopy (AFM) can provide information, which is in agreement with the above finding, and further, add unique information of the physical properties of cells that is impossible to obtain by other existing techniques. AFM indentation data was collected on individual cells, and subsequently, processed through the brush model to obtain information about the mechanics of the cell body (absolute values of the effective Young's modulus). Furthermore, information about physical properties of pericellular layer surrounding cells was obtained. We found a statistically significant decrease in the rigidity of mouse cells after the treatment, whereas there was no significant change found in the rigidity of NMR cells upon the treatment. We also found that the treatment caused a substantial increase in a long part of the pericellular layer in NMR cells only (the long brush was defined as having a size of >10 microns). The mouse cells and smaller brush did not show statistically significant changes upon the treatment.

The observed change of cell mechanics is in agreement with the frequently observed decrease of cell rigidity during progression towards cancer. The change of the pericellular layer due to malignant transformation of fibroblast cells has practically not been studied, though it was shown that removal of a part of the pericellular layer of NMR fibroblasts made the cells susceptible to malignant transformation. Although it is plausible to speculate that the observed increase of the long part of the brush layer of NMR cells might help cells to resist the malignant transformations, the significance of the observed change in the pericellular layer is yet to be understood. As of now, we can conclude that the change of cell mechanics might be used as an indication of the resistance of NMR cells to malignant transformations.

Keywords: cell mechanics, naked mole rats, genetic stability, atomic force microscopy, pericellular coat, brush model.

Introduction

Naked mole rats (NMR) exhibit an unusually long lifespan of up to 30 years, approximately nine times longer than mice [1-3]. It has also been accompanied by resistance to cancer [4, 5]. NMRs exhibit very little functional decline as they age, high fecundity until death, and no increase in mortality due to age [6]. Spontaneous cancer in NMR cells is very rare, and they are highly resistant to induced tumorigenesis [7, 8]. Researchers have linked this resistance to a variety of reasons. NMR secret hyaluronan acid (HA) 5-10 times larger in molecular mass compared to humans or mouse [9]. In addition, they exhibit resistance to oxidative stress, commonly linked to aging [10]. The NMR cells are sensitive to contact inhibition; cells arrest proliferation at a lower density relative to mouse fibroblasts [8].

Normal fibroblasts can be malignantly transformed by the introduction of a defined set of oncogenic hits, which include inactivation of tumor suppressors pRb and p53 and introduction of activated Ras oncogene RasV12 (Ras hereafter). SV40 Large T antigen (LT) is a viral oncoprotein that binds and inactivates pRb and p53 tumor suppressors [11], and is often used to experimentally

induce malignant transformation of cells. Mouse cells are malignantly transformed with high efficiency by a combination of LT and Ras. In contrast, NMR fibroblasts are resistant to malignant transformations with this set of factors and require either very high expression of Ras or abrogation of hyaluronan synthesis [12]. Furthermore, LT and Ras cause fewer transcriptional changes in NMR cells when compared to mouse cells [13].

Here we investigated physical changes of both NMR and mouse fibroblast cells upon the malignant transformations with LT and Ras. Atomic force microscopy (AFM) has become popular in studying the physical properties of cells [14-16], in particular, cell mechanics [17-19]. Correlation between elasticity of cells and different human diseases or abnormalities has been implicated in the pathogenesis of many progressive diseases, including vascular and kidney diseases, cancer, malaria, cataracts, Alzheimer, complications of diabetes, cardiomyopathies [17-22] and even aging [23-25].

In addition to the mechanics of the cell body, AFM can be used to obtain information about the pericellular coat, a layer consisting of glycocalyx molecules, and corrugation of the pericellular membrane. Mechanically, this layer resembles the behavior of polymer brush. As recently discovered, this pericellular brush (PB) layer is critical to understanding the overall cell mechanics [26] by providing not only additional information about the mechanics of the PB layer but also allowing to calculate the effective Young's modules in a more accurate self-consistent way. The latter is paramount when comparing results obtained on different microscopes and different labs. Furthermore, the brush model allows obtaining the parameters of physical properties of cells in the robust manner, i.e., weakly dependent on the uncertainties in the experimental data and model assumptions. As was recently shown, the errors in the definition of the effective Young's modulus due to possible uncertainties of the model and experimental data are within 4%, which is less than the error, for example, due to a typical uncertainty in the spring constant of the AFM cantilever [27]. The knowledge of the PB layer has a big biological significance. This layer surrounds neurofilaments to maintain interfilamentous spacing [28]. It is responsible for cell-cell interaction [29], cell migration [30], differentiation, and proliferation [31, 32]. The PB layer is important in embryonic development [33], wound healing [34], inflammation [35, 36], and mammalian fertilization [37]. It is involved in epithelial-mesenchymal transition [33], resistance to apoptosis (cell death), and multidrug resistance [38]. Furthermore, it has been demonstrated that the cell surface can be substantially changed as a result of genetic alterations [39].

In this work, we use the AFM technique to measure the physical properties of NMR and mouse fibroblasts in response to the malignant transformations using LT oncoproteins and Ras oncogene. Indentation force curves were collected with AFM. Cell geometry was taken into account to calculated the exact contact area between the AFM probe and cell. The collected force curves were processed with the brush model to study the alteration of cell mechanics and properties of pericellular coat surrounding the cells. We observed that the mechanics of the cell body of NMR cells changed insignificantly upon introduction of LT and Ras. At the same time, similar treatment of mouse cells did show a significant decrease in the rigidity of the mouse cell body. Such a change is in agreement with multiple works reporting softening of cells during progression towards cancer [19, 24, 40-43]. As to the precellular coat layer, the malignant transformations caused a substantial increase in the long part of the brush in NMR cells only (the long part was defined as having the size >10 microns). The other cells and smaller brush did not show statistically significant changes upon the malignant transformations. The change of the pericellular layer due to the malignant transformation of cells has not been studied for fibroblasts. Nevertheless, it was shown that a removal of a part of the pericellular layer of NMR fibroblasts made the cells susceptible to malignant transformation [12]. Although it is plausible to speculate that the observed increase of the long part of brush of NMR cells might help cells to resist the malignant transformations, the significance of the observed change in the pericellular layer is yet to be understood. Thus, as of now, we can conclude that the change of cell mechanics might be used as an indication of the resistance of NMR cells to malignant transformations.

Materials and Methods

Cells

Primary fibroblast cells were extracted from the skin tissue of animals by means of enzymatic digestion. The experiments were performed on cells at low passage numbers (population doubling 4-10). Cells were grown at 37^{o}C, 5% CO_2, and 5% O_2 on treated polystyrene culture dishes (Corning) using Eagle's Minimum Essential Medium (EMEM) supplemented with 15% FBS (Gibco) and 1% Penicillin-Streptomycin solution (Gibco) for 1-2 days. Cells were transported to the AFM lab in Corning flasks filled with culture media overnight without freezing. The amount of the growth medium in the flasks was close to the maximum possible to avoid mechanical damage of cells during

transportation. After receiving, the excessive medium was removed (only 10 ml of the media was kept in each flask). After transportation, flasks with cells were placed in an incubator at 37C (5% CO_2) for 12-16 hours. Before the AFM imaging, the top side of the culture bottles was removed. The AFM study was done directly in the medium on the cells attached to the bottom of the culture bottle. A relatively large amount of the medium insured the safety of the cell while imaging (ran about three hours; no statistical difference differences between the cell parameters derived from the measurements in the beginning and at the end of the experiments was noticed). The study of this work was done on cells close to confluency.

Atomic force microscopy

Dimension 3100 and Dimension Icon (Bruker Nano/Veeco, Inc.) AFMs with Nanoscope V controllers with nPoint (nPoint, Inc.) close-loop scanners (200 μm × 200 μm × 25 μm, XYZ) were used in the present study. It is important to stress that the use of such a large Z-range close-loop scanner is critical to detect a rather large brush layer. Standard cantilever holders for operation in liquids were used. The force curves were collected with a vertical ramp size up to 22 μm. To minimize viscoelastic (time-dependent) effects, force-indentation curves were collected with the fixed approach vertical speed of 27 μm/sec and retract speed of 120 μm/sec. The force-volume images of cells were collected with the resolution of 16x16 pixels within 50 x 50 μm^2 area for sparsely distributed cells and the resolution of 32x32 pixels within 150x150 μm^2 area for dense cells. A standard V-shaped arrow 200 μm AFM tipless cantilevers (Veeco, Santa Barbara, CA) were used throughout the study. A 5 μm diameter silica balls (Bangs Labs, Inc.) were glued to the cantilevers as described in [23]. A dull spherical probe is required to extract rigidity of the cell body in a self-consistent way [26]. Specifically, the elastic modulus of the analyzed force curves was near for different indentation depths [44, 45]. The radius of the probe (~2500nm) was measured by imaging the inverse grid (TGT1 by NT-NGT, Russia), see the supplementary materials for detail. The cantilever spring constant (~0.06 N/m) was measured using the thermal tuning method before gluing a silica ball.

It should be noted that a reliable detection of the outer part of the pericellular brush layer (called long or outer brush) may require an accurate recording of rather small forces. For example, it can be smaller than 100pN (see, Fig. S3c). Therefore, it is important to use the AFM setup that can hold the baseline (zero force) with sufficient accuracy. In the case of the used Dimension series of Bruker microscopes (3100 and Icon), it was attained by the use of an additional the nPoint scanner (commercially available add-on for Dimension series AFMs). The baseline was held at zero within 0.22 nm or 13pN (RMS) when the AFM tip is approaching the Petri dish surface from 7 to 1 μm (Figure S5). Closer than 1 μm, one can see a noticeable repulsion presumably due to hydrodynamic viscous squeezing out water between the AFM probe and sample. It is important to note that the chosen vertical approach speed of 27 μm/sec was chosen specifically to this effect small. If one interprets this hydrodynamic squeezing force as an effective brush layer, one can find the effective "size" of such brush (L^*N as defined later in the paper) to be very small compared to the cell brush (14 μm^{-1} versus 100-1000 μm^{-1}, see Figure 6). It allows us to ignore this effect. A possible influence of the bottom substrate under the measurements of the modulus is less than 12%, and therefore, is ignored in this work (see the supplementary materials for detail).

Data collection and processing

The force-volume mode of operation was utilized to obtain force curves over the cell surface and simultaneously record cell topography. While the approach and retract indentation curves are recorded by the AFM, only the approach curves are analyzed. This is because the retraction curves are subject to the complex relaxation behavior of cell deformation, and the approach curves are recorded over a relatively undisturbed surface.

The model described below was developed for a known geometry such as a sphere over either plane or hemisphere or sphere. Therefore, we consider only the force curves from the top area of cells (following the previous works [46-48]). This geometry can be approximated by the sphere-over-sphere configuration. We consider only the force curves on the cell surface around the top when the incline of the surface is less than 10-15 degrees. To identify such curves, the cell height image was used (this image was collected as a part of the force-volume data set). The angle of the incline was calculated using SPIP software (by Image Metrology, A/S). The radius of the cell curvature was derived from these images after correcting the cell heights for deformations, see ref. [49]

for detail; an example is given in supplementary materials, figure S5. On average, 4-5 force curves per cell were analyzed.

The brush model was used to process the force curves. A brief description of the Brush model is provided here, see [50, 51] for detail. Even more detail, including the robustness and error analysis of this model was presented in [27], where a high robustness of the model and relatively low error of the derived parameters were reported. Each force curve derived from the AFM is a function of the cantilever deflection (d) with respect to the vertical displacement of the AFM scanner (Z). A schematic of an AFM probe deforming a cell surface, which is covered with a pericellular brush layer, Fig. 1. The origin of Z is defined at the maximum deflection of the AFM cantilever (maximum indentation force), which gives the following relation between the geometrical parameters defined in Fig. 1:

$$h = Z - Z_0 + \left[\frac{9}{16}\frac{k}{E}\sqrt{\frac{R_{probe}+R_{cell}}{R_{probe}R_{cell}}}\right]^{2/3} d^{2/3} + d \qquad (1)$$

where Z_0 is the position of the undeformed cell body, h is the distance between the AFM probe and the surface of the cell body, E is the elastic (Young's) modulus, k is the spring constant of the AFM cantilever, and R probe (R cell) are the radius of the AFM probe (cell). The Poisson ratio of a cell is chosen to be 0.5. Because of a small range of possible variations of the Poisson ratio, the error due to the uncertainty of its definition is small.

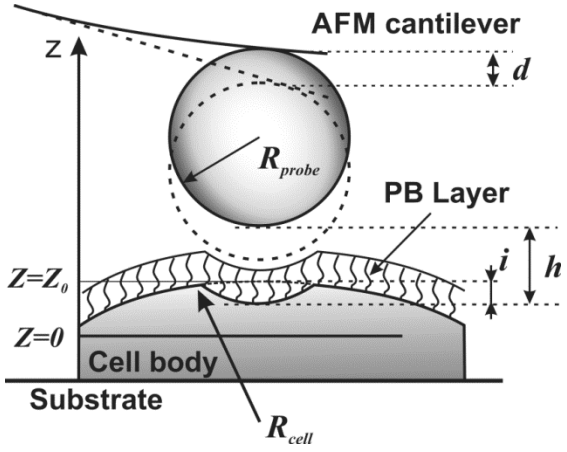

Figure 1. A schematic of an AFM spherical indenter (probe) deforming a biological cell. ***Z*** is the vertical position of the AFM scanner, ***d*** is the AFM cantilever deflection, $\boldsymbol{Z_0}$ is the position of an undeformed cell body, ***i*** is the deformation of the cell body, ***Z***=0 is assigned to the maximum force, and ***h*** is the distance between the cell body and AFM probe.

It should be noted that the Hertz model used in equation 1 is based on the assumption that the thickness of the cell body is much greater than the indentation depth. In the present work, this assumption is valid. The average thickness of the cells (derived from the force volume images, see the supplementary materials), was ~10 microns, whereas the indentation depth was ~0.5 microns.

The raw force curve (*d* vs *Z*) requires two steps to be processed. In step 1, the curve is used to determine the effective Young's modulus of the cell body. After some initial deformation, a portion of the force curve can be assumed to have a fully squeezed PB layer, or *h*=0. Because the adhesion force between the probe and cell surface is either absent or negligible compared to the indention force, the Hertz contact model can be used [45] in this step. The effective Young's modulus can then be determined from fitting this maximum deflection portion of the curve with equation (1), in which *h*=0, and undeformed position of the cell body (Z_o) is treated as a free unknown parameter. A graphical example of such processing is shown in Fig.2 (left). It should be noted that due to intrinsic inhomogeneity of the cell body, the self-consistency of the above approach can be verified by calculating the values of the Young's modulus and different penetration depths. The depth independence indicates the sought self-consistency, see [50, 52, 53] for detail.

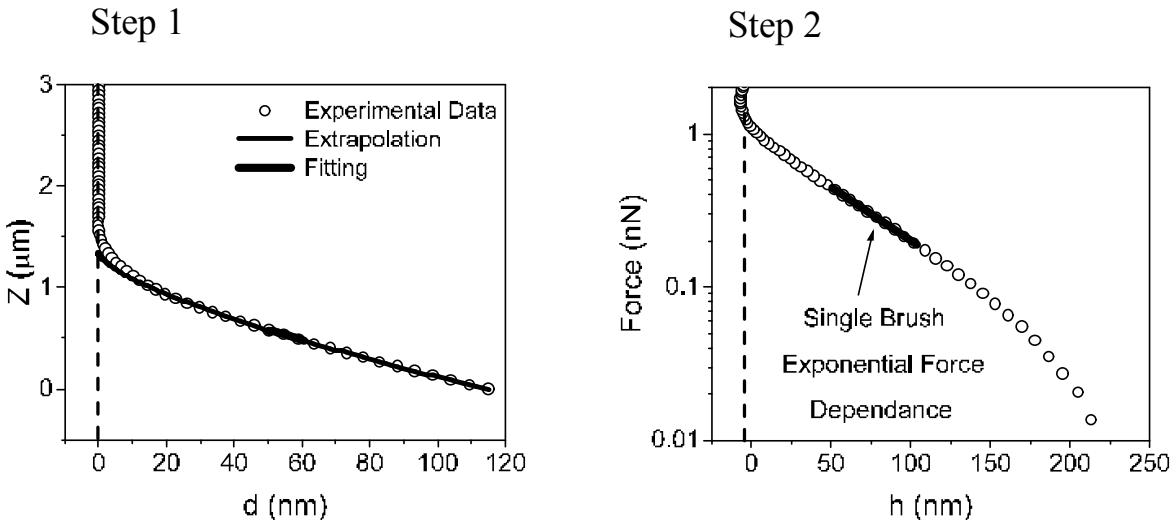

Figure 2. An example of processing of an indentation force curve through the brush model. The experimental data are shown with open circles. Step 1 (left) shows the fitting which defines the effective Young's modulus of the cell body (assuming a fully squeezed pericellular brush layer). Step 2 (right) displays the derived force due to the brush layer as a function of the distance between the AFM probe and cell surface. One can see the exponential force dependence (straight line in the logarithmic force scale).

In step 2, the parameters of the pericellular brush layer (effective grafting density and brush length) are determined. Equation (1) is used to determine *h(d)*, where the values of E and Z_0 are no longer unknown and defined at the previous step. The derived curve represents the force due to exclusively the pericellular brush layer. Plotting this force in the logarithmic scale will show a linear straight slope, indicating exponential force-distance dependence in this portion of indentation. Such force dependences are typical for the indentation of entropic polymer brushes and/or surfaces with random asperities. To describe the parameters of this layer, the following equation is used for the force of steric interaction between a spherical probe and a semi-spherical cell [32,34,35]:

$$F(h) \approx 100 k_B T R^* N^{3/2} exp\left(-2\pi \frac{h}{L}\right) L \ , \qquad (2)$$

where k_B is the Boltzmann constant, T is the temperature, N is the surface density of the brush constituents (grafting density, effective molecular density), $R^* = R_{probe} \cdot R_{cell} / (R_{probe} + R_{cell})$, and L is the equilibrium thickness of the PB layer. This formula it is valid provided $0.1 < h/L < 0.8$.

In multiple cases, the force due to brush does not show a single exponential behavior. It is rather well described by a double exponential behavior [46, 54]. This represents "inner" and "outer" parts of the PB layer. The inner brush is mainly defined by the corrugation of the pericellular membrane described in biology as microridges and microvilli. The outer brush is mainly defined by long polysaccharide molecules of glycocalyx surrounding the cell [49]. The brush is assumed to consist of two characteristic length and grafting densities, corresponding to the shorter and more rigid inner brush, and the longer and assumedly softer outer brush. The force due to the double-sized brush layer is well parameterized by the following equation [49]:

$$F(h) \approx 100 k_B T R^* \left(N_1^{3/2} \exp\left(-2\pi \frac{h}{L_1}\right) L_1 + N_2^{3/2} \exp\left(-2\pi \frac{h}{L_2}\right) L_2\right) \qquad (3)$$

where N_1, L_1, and N_2, L_2 are the parameters of the outer and inner brush, respectively.

It should be noted that the above models describe the situation of the static measurements. In the same time, as was shown in [49], the measured parameters of the brush layer depend on the indentation speed. The use of the static approximation is justified by the present state of the art. For example, the Young's modulus is a static one, and strictly speaking, it should be measured infinitely slowly. Nevertheless, it cannot be measured with a very low speed of indentation because cells are active material. It can be changed during the measurements if the measurements are done too slowly. The presently used speeds are a compromise between the time of the measurements and relatively slow speed. It is worth noting that in principle, one can take into account the indentation speed and calculate time-dependent (visco- or poro- elastic) properties of the cell body. However, the best of the authors knowledge, there is no time-dependent theory of the polymer brush exist at the moment. Therefore, to study the changes of the cells studied in this work, we keep exactly the same speeds of indentation for all groups of cells considered in our work.

It is also important to note that the approach speed of the sample and AFM probe was chosen to avoid a noticeable hydrodynamic (viscous) effect. A representative force curve approaching the petri dish surface (away from cells) is shown in figure S4 of the supplementary material. One can see almost no viscous effect when approaching the surface. A possible influence of the bottom substrate under the measurements of the modulus at less than 12%, and therefore is ignored in this work (see the supplementary materials for detail).

Statistical analysis

Two sample variance test was done to compare the distribution of data of the control to each modification. If population variances were similar, the ANOVA test was used to determine the statistical significance of the observed difference. If population variance was significantly different, the non-parametric Mann-Whitney test was used to determine if the difference is significant. Hereafter, the statistical significance p is marked in all graphs with * ($p < 0.05$), ** ($p < 0.01$), *** ($p < 0.001$).

Results

Naked mole rat (NMR) and mouse fibroblast cells were analyzed using the brush model described in the Methods section. The derived modulus, brush length, and brush density values were then compared between control (wild type) and genetically modified cells (LT and LT-Ras modifications).

Examples of data processing are shown in the supplementary materials. The average height of NMR cells was 8.5 μm and 6 μm for mouse cells. Indentation depth (of the cell body) used to calculate the Young's modulus were ~0.5 microns. Therefore, the bottom effect was negligible. The curvature radius of the top part of the cells was at a range of 9.0 – 160 μm (NMR) and 6.0 – 170 μm (mouse). Figure 3 shows the results for the effective Young's modulus calculated for mice and NMR. A significant decrease in stiffness of mouse fibroblast cells due to genetic modification is not reciprocated in the NMR fibroblast cells. The derived modulus values for control and modified NMR (left) and mouse (right) cells are represented by the mean and one standard deviation. One can see that the NMR cells show no significant change in the modulus due to either of the genetic modifications. At the same time, the mouse cells demonstrate a significant decrease of 1.9 times in modulus with the LT modification and a decrease of 2.7 times with the LT-Ras modification.

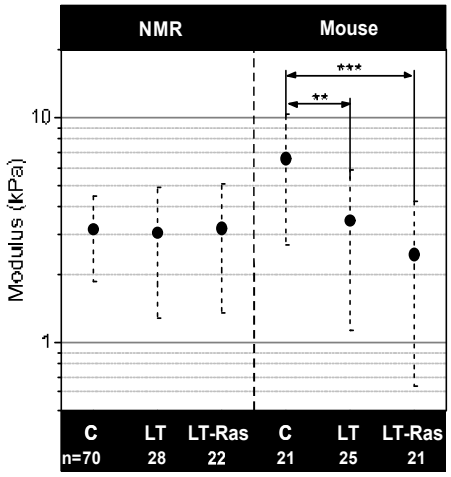

Figure 3. The values of the effective Young's modulus calculated for mice and naked mole rats. The mean value and one standard deviation are shown. The abbreviations in the bottom: C stands for the control (wild) cell type, LT is for LT modification, LT-Ras is for LT-Ras

modification. The number of tested cells is shown at the bottom of the graph. The statistical significance p is marked in this graph with ** ($p < 0.01$), *** ($p < 0.001$).

The analysis of the forces due to the PB layer shows that some force curves demonstrate a single brush behavior whereas the other curves show the double brush behavior within the same cell. Roughly 50% of NMR control, 21% of NMR LT, 78% of NMR LT-Ras, 81% of mouse control, 60% of mouse LT, and 29% of mouse LT-Ras cells have at least one force curve with the double brush behavior. It is constructive to compare the behavior of these two types of brush separately. Figure 4 shows the results for the single brush only. One can see that the NMR single brush is shortened by approximately 1.3 times with the LT-Ras transformation. When comparing the grafting density of the PB layer, the NMR cells are significantly affected by the genetic modification. Both LT and LT-Ras modification significantly increase the brush density of the NMR cells, by 6.1 and 3.2 times, respectively. However, the mouse cells show no significant change in density relative to the control.

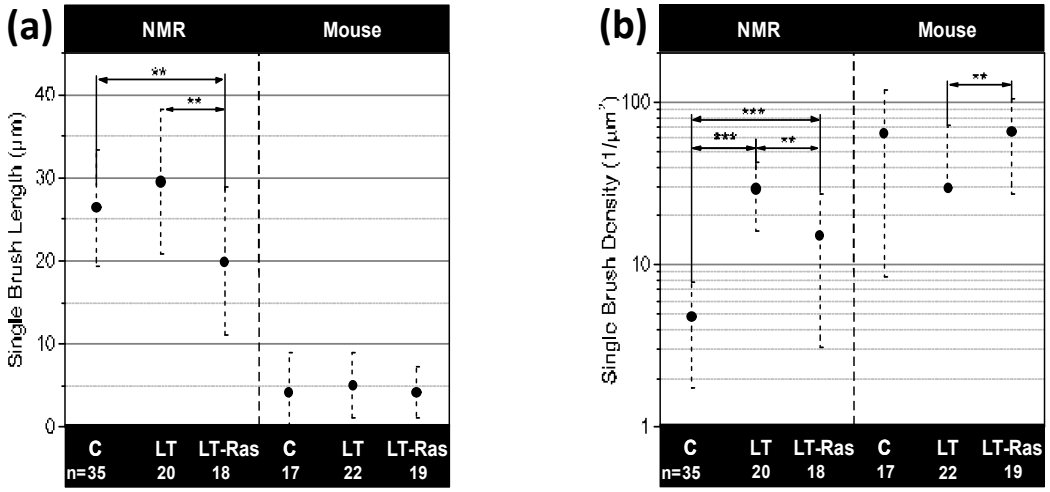

Figure 4. The parameters of the single-brush layer calculated for mice and NMR cells: a) the brush length and b) grafting density of the pericellular brush layer. The mean value and one standard deviation are shown. The abbreviations in the bottom: C stands for the control (wild) cell type, lt is for LT genetic modification, LT-Ras is for LT-Ras modification. The

number of tested cells is shown at the bottom of the graph. The statistical significance p is marked in this graph with ** ($p < 0.01$), *** ($p < 0.001$).

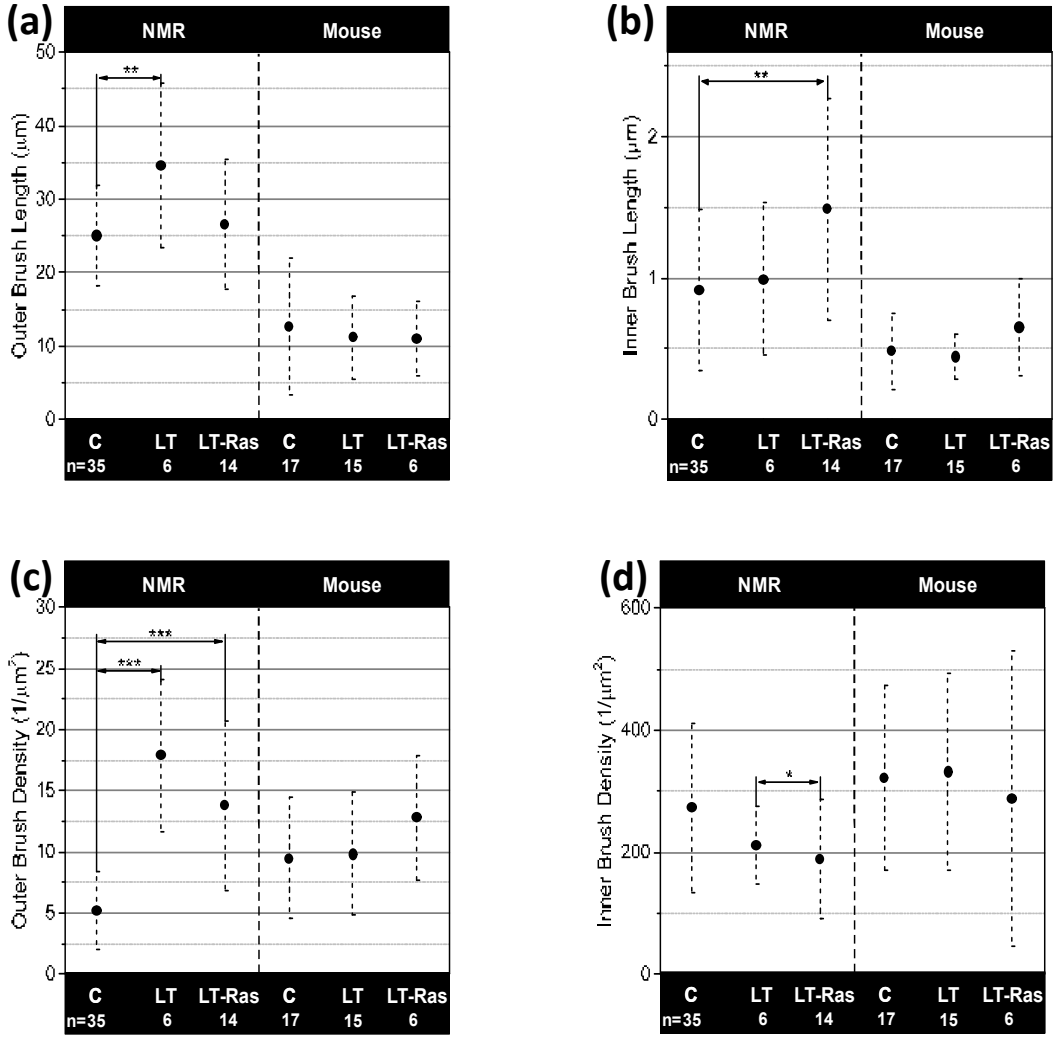

Figure 5. The parameters of the double-brush layer calculated for mice and NMR cells: the brush length for the outer (a) and inner (b) brush, and the grafting density of the outer (c) and inner (d) pericellular brush layer. The mean value and one standard deviation are shown. The abbreviations in the bottom: C stands for the control (wild) cell type, lt is for LT genetic modification, lt-Ras is for LT-Ras modification. The number of tested cells is shown at the bottom of the graph. The statistical significance p is marked in this graph with * ($p < 0.05$), ** ($p < 0.01$), *** ($p < 0.001$).

Figure 5 presents the results of processing double-brush force curves. Because for some cell types the number of such force curves is low, the statistical significance has to be considered rather cautiously. One can see that NMR outer brush length changes due to lt modification by about 1.4 times. LT-Ras elongates the inner brush by about 1.6 times. NMR outer brush density changes significantly with both modifications, by 3.4 and 2.6 times, respectively. Inner brush density does not show significant changes for NMR cells compared to control. It is important to note that only six cell samples were categorized as NMR LT-modified double brush; thus, this level of significance could be due to a small population of the sample. Mouse cells show no significant changes in the double brush.

Discussion

One can see in the obtained results that the malignant modification does not make any statistically significant changes in the mechanics of the NMR cell body, whereas the mechanical properties of mouse cells decrease substantially. As shown in multiple publications [24, 41, 42, 55], the decrease of the cell stiffness correlates well with the progression towards cancer. One of the key distinctive features of NMR is their overall longevity and resistance to cancer. So the observed results vote in favor that the considered malignant modifications do not lead to the development of cancer in NMR. At the same time, the stiffness of mouse cells drops after the malignant modifications as expected for malignant cells. So, we can speculate that AFM can be used to identify malignant modifications that could lead to the conversion of normal cells to cancerous. Nevertheless, it should be noted that the malignant cells are not always softer than normal cells. For example, no statistically significant difference between rigidities of cancer and normal cells was reported for human cervical epithelial cells during progression towards cancer [46]. To be precise, normal cells studied in that work were grown in the culture medium, which contained a higher concentration of human growth factors. This was done to mimic the case of normal cells in a reactive tissue (the tissue formed under inflammation or irritation). Geometry of cells grown under such conditions becomes very similar to the geometry of malignant cells. As a result, normal and cancerous cells were almost identical under an optical microscope. In contrast, virtually all previous works, which

reported the differences in mechanics of malignant and normal cells, were performed using “regular” normal cells that had different geometry seen under a regular optical microscope.

NMR cells demonstrate a statistically significant change in the size of the PB layer. Both NMR and mouse cells show changes in the grafting densities of the PB layer for both single and double brush cell types. NMR cells, however, demonstrate a more consistent increase of the combined brush length and density with the malignant modifications. Fig.6 demonstrates it by presenting an integral parameter representative of the total amount of the brush, which is a product of the brush length and grafting density. If applied to the polymer brush model, such a parameter gives the total effective length of all molecules of the brush layer per unit area. We found that there is a statistically significant increase in the brush part/layer, which size was greater than 10 μm. For simplicity, we call it “long brush”, and the rest is “short brush”. The long brush comprises the outer brush in the case of double brush, and in the case of a single brush. One can see from Fig.6a that NMR cells show a substantial increase of the long brush with LT and LT-Ras modification, by 7.1 and 2.9 times, respectively. Mouse cells do not show any statistically significant change of the long brush. As was shown before using guinea pig fibroblast cells [49], the long brush comprises long polysaccharide molecules of glycocalyx, presumably hyaluronic acid.

To the best of the authors' knowledge, the physical properties of the pericellular brush layer during malignant transformations have not been studied for fibroblast cells. As was shown for an example of human cervical epithelial cells, the decrease in the size and grafting density of the outer brush layer correlated with the malignancy of those cells [46]. However, the outer layer of those cells had a size of ~2μm, which is more similar to the inner layer of both NMR and mouse fibroblasts. Furthermore, biochemical analysis of hyaluronic acid, one of the major components of the pericellular brush layer, shows a very complicated correlation between hyaluronic acid and progression to cancer. The size-dependent biological functions of hyaluronic acid add to the complexity of possible analysis [12, 56]. Dealing with NMR cells, one deals with a very high-molecular weight hyaluronic acid (vHMW HA, > 6000 kDa), which is unique to NMR. As was shown [12], the enzymatic removal of this hyaluronic layer made NMR cells susceptible to malignant transformation. So it seems to be plausible to speculate that the observed increase of the long brush of NMR cells may correlate with the increase of vHMW hyaluronic component of the pericellular layer. And this might help to decrease the chances of NMR cells becoming malignant. To address this hypothesis, further studies are needed.

In conclusion, it is worth noting that the obtained results are not only in obtaining a new knowledge about physical properties of age- and cancer- resistant cells. We also expect that the results presented in this work will further expand the interest in atomic force microscopy and demonstrate that this technique allows obtaining unique information, which might be used to shed light on the longevity and resistance to cancer.

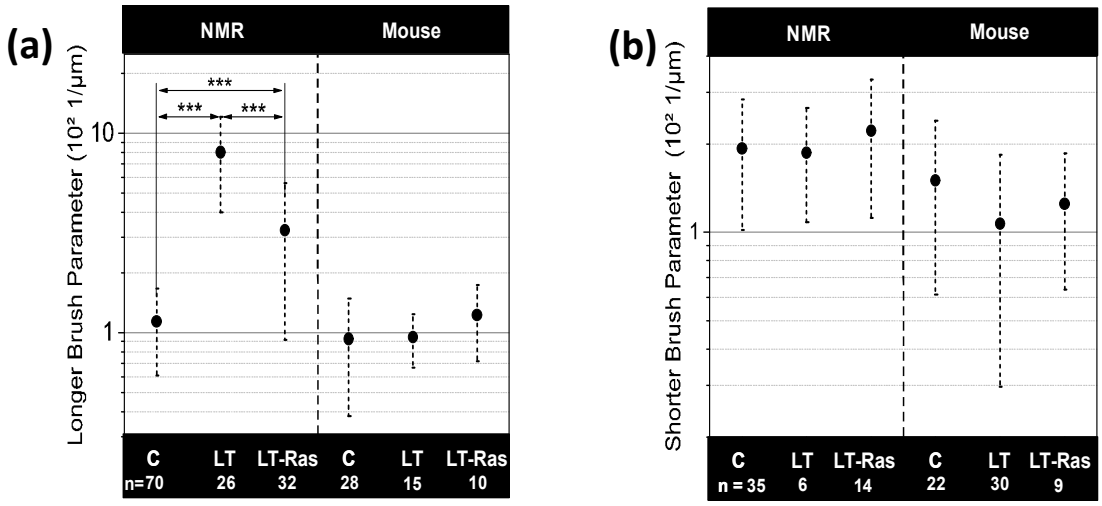

Figure 6. The L*N parameter for the brush layer calculated for NMR and mice cells: both for the longer (a) and shorter (b) brush. The mean value and one standard deviation are shown. The abbreviations in the bottom: C stands for the control (wild) cell type, LT is for LT genetic modification, LT-Ras is for LT-Ras modification. The number of tested cells is shown at the bottom of the graph. The statistical significance p is marked in this graph with ** ($p < 0.01$), *** ($p < 0.001$).

Author Contributions

I.S. and V.G. designed and supervised the work; A.S., V.G. prepared samples; V.K., M.D. conducted the AFM measurements; M.D., N.M. and V.K. processed the data; I.S., V.G. and M.D. analyzed

the data; N.M. and I.S. prepared figures, N.M. and I.S. drafted the manuscript; all authors discussed the results and commented on the manuscript.

Acknowledgements

This work was funded by NSF grant CMMI 1435655 (I.S.) and US National Institutes of Health, Institute of Aging grants (P01 AG047200-03) to A.S. and V.G, and by Life Extension Foundation to A.S. and V.G.

Conflict of interest

The authors declare that they have no conflict of interest. The findings and conclusions in this report are those of the authors and do not necessarily represent the views of the National Science Foundation and the National Institutes of Health.

Cited literature

1. R. Buffenstein, *The Journals of Gerontology Series A: Biological Sciences and Medical Sciences*, 2005, **60**, 1369-1377.
2. Y. H. Edrey, M. Hanes, M. Pinto, J. Mele and R. Buffenstein, *ILAR Journal*, 2011, **52**, 41-53.
3. E. B. Kim, X. Fang, A. A. Fushan, Z. Huang, A. V. Lobanov, L. Han, S. M. Marino, X. Sun, A. A. Turanov, P. Yang, S. H. Yim, X. Zhao, M. V. Kasaikina, N. Stoletzki, C. Peng, P. Polak, Z. Xiong, A. Kiezun, Y. Zhu, Y. Chen, G. V. Kryukov, Q. Zhang, L. Peshkin, L. Yang, R. T. Bronson, R. Buffenstein, B. Wang, C. Han, Q. Li, L. Chen, W. Zhao, S. R. Sunyaev, T. J. Park, G. Zhang, J. Wang and V. N. Gladyshev, *Nature*, 2011, **479**, 223-227.
4. J. Jarvis *Journal of Zoology*, 2002, **258**, 307-311.

5. M. Keane, T. Craig, J. Alfoldi, A. M. Berlin, J. Johnson, A. Seluanov, V. Gorbunova, F. Di Palma, K. Lindblad-Toh, G. M. Church and J. P. De Magalhaes, *Bioinformatics*, 2014, **30**, 3558-3560.
6. R. Buffenstein, *J Comp Physiol B*, 2008, **178**, 439-445.
7. S. Liang, J. Mele, Y. Wu, R. Buffenstein and P. J. Hornsby, *Aging Cell*, 2010, **9**, 626-635.
8. A. Seluanov, C. Hine, J. Azpurua, M. Feigenson, M. Bozzella, Z. Mao, K. C. Catania and V. Gorbunova, *Proceedings of the National Academy of Sciences*, 2009, **106**, 19352-19357.
9. X. Tian, J. Azpurua, C. Hine, A. Vaidya, M. Myakishev-Rempel, J. Ablaeva, Z. Mao, E. Nevo, V. Gorbunova and A. Seluanov, *Nature*, 2013, **499**, 346-349.
10. V. I. Perez, R. Buffenstein, V. Masamsetti, S. Leonard, A. B. Salmon, J. Mele, B. Andziak, T. Yang, Y. Edrey, B. Friguet, W. Ward, A. Richardson and A. Chaudhuri, *Proceedings of the National Academy of Sciences*, 2009, **106**, 3059-3064.
11. W. C. Hahn, S. K. Dessain, M. W. Brooks, J. E. King, B. Elenbaas, D. M. Sabatini, J. A. DeCaprio and R. A. Weinberg, *Mol Cell Biol*, 2002, **22**, 2111-2123.
12. X. Tian, J. Azpurua, C. Hine, A. Vaidya, M. Myakishev-Rempel, J. Ablaeva, Z. Mao, E. Nevo, V. Gorbunova and A. Seluanov, *Nature*, 2013, **499**, 346-349.
13. J. Zhao, X. Tian, Y. Zhu, Z. Zhang, E. Rydkina, Y. Yuan, H. Zhang, B. Roy, A. Cornwell, E. Nevo, X. Shang, R. Huang, K. Kristiansen, A. Seluanov, X. Fang and V. Gorbunova, *Nature*, 2020, **583**, E8-E13.
14. Y. F. Dufrene, D. Martinez-Martin, I. Medalsy, D. Alsteens and D. J. Muller, *Nature Methods*, 2013, **10**, 847-854.
15. T. Berdyyeva, C. D. Woodworth and I. Sokolov, *Ultramicroscopy*, 2005, **102**, 189-198.
16. I. Sokolov, S. Iyer, V. Subba-Rao, R. M. Gaikwad and C. D. Woodworth, *Applied Physics Letters*, 2007, **91**, 023902.
17. N. Makarova, V. Kalaparthi, A. Wang, C. Williams, M. E. Dokukin, C. K. Kaufman, L. Zon and I. Sokolov, *J Mech Behav Biomed*, 2020, **107**, 103746.
18. P. H. Wu, D. R. B. Aroush, A. Asnacios, W. C. Chen, M. E. Dokukin, B. L. Doss, P. Durand-Smet, A. Ekpenyong, J. Guck, N. V. Guz, P. A. Janmey, J. S. H. Lee, N. M. Moore, A. Ott, Y. C. Poh, R. Ros, M. Sander, I. Sokolov, J. R. Staunton, N. Wang, G. Whyte and D. Wirtz, *Nature Methods*, 2018, **15**, 491-498.

19. M. Lekka, P. Laidler, D. Gil, J. Lekki, Z. Stachura and A. Z. Hrynkiewicz, *Eur Biophys J*, 1999, **28**, 312-316.
20. R. Bucala and A. Cerami, *Adv Pharmacol*, 1992, **23**, 1-34.
21. R. J. Castellani, P. L. Harris, L. M. Sayre, J. Fujii, N. Taniguchi, M. P. Vitek, H. Founds, C. S. Atwood, G. Perry and M. A. Smith, *Free Radic Biol Med*, 2001, **31**, 175-180.
22. P. Ulrich and X. Zhang, *Diabetologia*, 1997, **40**, S157-S159.
23. T. K. Berdyyeva, C. D. Woodworth and I. Sokolov, *Phys Med Biol*, 2005, **50**, 81-92.
24. S. Suresh, *Acta Biomater*, 2007, **3**, 413-438.
25. J. T. Zahn, I. Louban, S. Jungbauer, M. Bissinger, D. Kaufmann, R. Kemkemer and J. P. Spatz, *Small*, 2011, **7**, 1480-1487.
26. N. Guz, M. Dokukin, V. Kalaparthi and I. Sokolov, *Biophysical Journal*, 2014, **107**, 564-575.
27. N. Makarova and I. Sokolov, *Nanoscale*, 2022, **14**, 4334-4347.
28. H. G. Brown and J. H. Hoh, *Biochemistry*, 1997, **36**, 15035-15040.
29. R. Kosaki, K. Watanabe and Y. Yamaguchi, *Cancer Res*, 1999, **59**, 1141-1145.
30. N. Itano, F. Atsumi, T. Sawai, Y. Yamada, O. Miyaishi, T. Senga, M. Hamaguchi and K. Kimata, *Proc Natl Acad Sci U S A*, 2002, **99**, 3609-3614.
31. E. Zimmerman, B. Geiger and L. Addadi, *Biophys J*, 2002, **82**, 1848-1857.
32. B. P. Toole, *Cell Biology of the Extracellular Matrix*, Plenum Press, E Hay edn., 1982.
33. T. D. Camenisch, J. A. Schroeder, J. Bradley, S. E. Klewer and J. A. McDonald, *Nature Medicine*, 2002, **8**, 850-855.
34. W. Y. Chen and G. Abatangelo, *Wound Repair Regen*, 1999, **7**, 79-89.
35. C. A. de la Motte, V. C. Hascall, J. Drazba, S. K. Bandyopadhyay and S. A. Strong, *Am J Pathol*, 2003, **163**, 121-133.
36. D. Jiang, J. Liang, J. Fan, S. Yu, S. Chen, Y. Luo, G. D. Prestwich, M. M. Mascarenhas, H. G. Garg, D. A. Quinn, R. J. Homer, D. R. Goldstein, R. Bucala, P. J. Lee, R. Medzhitov and P. W. Noble, *Nat Med*, 2005, **11**, 1173-1179.
37. J. S. Richards, *Mol Cell Endocrinol*, 2005, **234**, 75-79.
38. B. P. Toole, *Nat Rev Cancer*, 2004, **4**, 528-539.
39. S. Prasad, A. Rankine, T. Prasad, P. Song, M. E. Dokukin, N. Makarova, V. Backman and I. Sokolov, *Advanced NanoBiomed Research*, 2021, DOI: 10.1002/anbr.202000116, 2000116.
40. A. Stylianou, M. Lekka and T. Stylianopoulos, *Nanoscale*, 2018, **10**, 20930-20945.

41. L. Bastatas, D. Martinez-Marin, J. Matthews, J. Hashem, Y. J. Lee, S. Sennoune, S. Filleur, R. Martinez-Zaguilan and S. Park, *Biochim Biophys Acta*, 2012, **1820**, 1111-1120.
42. S. E. Cross, Y. S. Jin, J. Tondre, R. Wong, J. Rao and J. K. Gimzewski, *Nanotechnology*, 2008, **19**, 384003.
43. I. Sokolov, *Atomic force microscopy in cancer cell research*, American Scientific Publishers' Inc, 2007.
44. H.-J. Butt, M. Kappl, H. Mueller, R. Raiteri, W. Meyer and J. Rühe, *Langmuir*, 1999, **15**, 2559-2565.
45. H. Hertz, 1882, **1882**, 156-171.
46. S. Iyer, R. M. Gaikwad, V. Subba-Rao, C. D. Woodworth and I. Sokolov, *Nature Nanotechnology*, 2009, **4**, 389-393.
47. I. Sokolov, S. Iyer, V. Subba-Rao, R. Gaikwad and C. Woodworth, *Applied Physics Letters*, 2007, **91**, 023902.
48. I. Sokolov, S. Iyer and C. D. Woodworth, *Nanomedicine: Nanotechnology, Biology and Medicine*, 2006, **2**, 31-36.
49. M. Dokukin, Y. Ablaeva, V. Kalaparthi, A. Seluanov, V. Gorbunova and I. Sokolov, *Biophysical Journal*, 2016, **111**, 236-246.
50. I. Sokolov and M. E. Dokukin, *Methods Mol Biol*, 2018, **1814**, 449-468.
51. I. Sokolov, M. E. Dokukin and N. V. Guz, *Methods*, 2013, **60**, 202-213.
52. Y. Liu, I. Sokolov, M. E. Dokukin, Y. Xiong and P. a. Peng, *Nanoscale*, 2020, **12**, 12432-12443.
53. N. Makarova, V. Kalaparthi, A. Wang, C. Williams, M. E. Dokukin, C. K. Kaufman, L. Zon and I. Sokolov, *J Mech Behav Biomed Mater*, 2020, **107**, 103746.
54. M. Dokukin, Y. Ablaeva, V. Kalaparthi, A. Seluanov, V. Gorbunova and I. Sokolov, *Biophys J*, 2016, **111**, 236-246.
55. Q. S. Li, G. Y. Lee, C. N. Ong and C. T. Lim, *Biochem Biophys Res Commun*, 2008, **374**, 609-613.
56. A. G. Tavianatou, I. Caon, M. Franchi, Z. Piperigkou, D. Galesso and N. K. Karamanos, *FEBS J*, 2019, **286**, 2883-2908.